*Refereed Proceedings*

*The 13th International Conference on Fluidization - New Paradigm in Fluidization Engineering*

Engineering Conferences International *Year* 2010

# FAST X-RAY TOMOGRAPHY OF A BUBBLING FLUIDIZED

Robert Frank Mudde
Delft University of Technology, r.f.mudde@tudelft.nl

# Fast X-Ray Tomography of a Bubbling Fluidized Bed

R.F. Mudde*
Kramers Laboratorium voor Fysische Technologie
Delft University of Technology
Pr.Bernhardlaan 6, 2628 BW Delft, The Netherlands.

**Abstract**

This paper presents results of a train of bubbles moving through a fluidized bed imaged with an X-ray Tomographic Scanner. The scanner consists of three X-ray sources equipped with 2*30 $CdWO_4$ detectors each. The fluidized bed has a diameter of 23cm and is filled with polystyrene particles (mean diameter 560$\mu$m). The bed is set at minimal fluidization and additional gas is released from a single capillary, forming a train of bubbles moving upwards through the bed. The scanner measures the shape, size and velocity of the bubbles passing the measuring plane. We present data showing that the scanner can quantify for each bubble its size and velocity. The smallest bubbles detected have an equivalent diameter of less than 3cm.

Key words: X-ray tomography, time resolved, spatial resolution, SART, bubbling fluidized bed

## 1 Introduction

Fluidization is a key operation in many chemical engineering application. Despite it being used for decades, still fluidization has not given up all its secrets and design, operation and scale-up of fluidized reactors remains a challenge. One of the reasons is in the difficulty encountered when performing hydrodynamic experiments. The well-known laser based techniques, like Laser Doppler Anemometry (LDA) or Particle Image Velocimetry (PIV) are practically useless in dense multi phase systems. Alternatives are Electrical Capacitance Tomography (ECT), Magnetic Resonance Imaging (MRI) or nuclear densitometry that can provide tomographic reconstructions of the density distribution inside the fluidized bed. ECT is a relatively cheap and fast technique, giving a high temporal resolution. Images can be produced at rates of several hundreds per second (see e.g. (1), (2), (3)). Recently, Fan and co-workers have used neural networks and a multi-criterion optimization to increase the spatial resolution (4). Moreover, they used a double ring of sensors, which allowed them to extend their technique to 3D reconstructions of a bubble plume (5). However, ECT works with so-called soft fields: a change in the electro-magnetic properties in one location changes the field everywhere in the domain. This makes reconstruction difficult and the resolution the center of the

*e-mail: r.f.mudde@tudelft.nl

object is usually relatively poor. Magnetic Resonance Imaging (MRI) in multiphase reactors is developed in the group of Gladden (6). It is based on the magnetic moment of a nuclear particle, like a proton. It can measure simultaneously velocities and spatial distributions, making it a complete technique. However, very strong magnets are required, limiting at present the possible diameter of the vessel to several centimeters. This is rather small for research on fluidized beds.
However, solids are to some extend transparent to radiation such as $X$ or $\gamma$ rays and a variety of nuclear techniques has been developed during the last decade. In (7) the use of nuclear techniques in opaque multiphase systems is reviewed. Radiation can be used to measure the volume fraction of gas (or equivalent of the solids) in a fluidized bed. If tomographic techniques are used, the volume fraction distribution in a cross section of the fluidized bed can be found. This is referred to as 'nuclear densitometry'. Several papers have appeared in literature, not only dealing with densitometry in fluidized beds, see e.g. (8), (9). For instance, (10) measured the volume fraction in a 48cm-diameter bubble column, using a single beam-detector pair to perform horizontal, uni-directional scans over a cross-sectional plane assuming cylinder symmetry. (11) followed a similar procedure to measure the solids volume fraction in a turbulent fluidized bed. (8) reported the use of a fan beam from a single $\gamma$ source with multiple detectors. By rotating the source-detector combination around the column about 4000 projections could be taken, resulting in a spatial resolution of 5mm. As the total measuring time is about one hour, a time averaged volume fraction is obtained. This type of tomographic reconstruction is referred to as Computed Tomography or CT. In medical imaging, the use of $X$-ray tomography is standard practice. The source-detector system again rotates around the patient. This way high resolution, static images can be produced.
Fast X-ray tomographic systems can be made by using e.g. multiple X-ray sources simultaneously. An other option is to generate the X-rays by moving an electron beam over a Tungsten element, see e.g. (12), (13). They can create tomographic images up to a rate of 10,000 frames/s. This is evidently showing that nuclear techniques can also be fast.
In the present paper, we report experiment using a three source $X$-rays scanner and a 23cm fluidized bed. We study a train of bubbles rising upwards through a fluidized bed operated at minimal fluidization.

## 2 Experimental Setup

A 23cm inner-diameter perspex tube (wall thickness 5mm) forms the fluidized bed. It is filled with 0.56mm sized polystyrene particles (solids density 1102 kg/m$^3$). This is a Geldart B powder. The minimum fluidization velocity is 0.12m/s. The air (room temperature) is via a wind box supplied to the bed through a porous plate (sintered bronze, pore size 30 to 70$\mu$m, plate thickness 7mm). The ungassed bed height is 59cm. A schematic of a fluidized bed with two bubbles in the measuring plane of the densitometer is given in Figure 1(a).
The $X$-ray sources are placed at 120$^\circ$ around the fluidized bed. Each source generates a fan beam that is detected by two sets of 32 sensors placed opposite of the source. By using 2 sets, two measuring planes are formed. The distance between the planes is about 1.9cm. Comparing the raw signals allows estimation of the velocity of passing bubbles and from that the bubble size in the vertical direction. A photo of the scanner is shown in Figure 1(b). The distance from the X-ray-target to the center of the fluidized

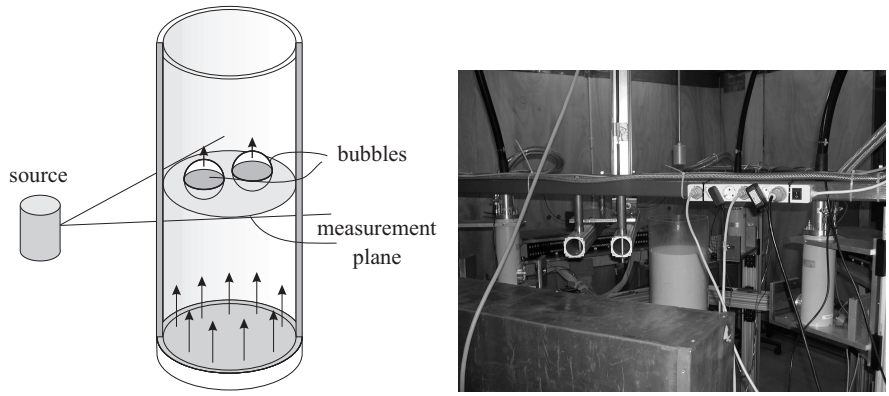


(a) Two bubbles in the measuring plane of the X-ray densitometer.

(b) Photo of the tomographic X-ray scanner.

Figure 1: Experimental Set-up

bed is 68.5cm, from the X-ray target to the detectors is 138.6cm. The fluidized bed is placed on a table that can be moved up and down in the vertical direction. This way we can adjust the height of the measuring plane in the column.
The X-ray sources used are manufactured by Yxlon International GmbH. The maximum X-ray energy is 150keV. We operate the sources at a low energy flux with a tube current less than 1mA. The detectors all consist of a $CdWO_4$ scintillation crystal optically coupled to a PIN photo diode. They are manufactured by Hamamatsu (type: S 1337 - 1010BR). Their crystal size is 10mm*10mm*10mm.
A plastic casing in the form of an arc holds two horizontal arrays of 32 detectors. The curvature of the array is such that the distance to the focal point of the source is equal for all detectors. Of these detectors 30 are used to produce data for tomographic reconstruction, the two outermost detectors are used to monitor the alignment of the object vessel and proper functioning of the tomographic system. The data are collected simultaneously at a sampling frequency of 2500Hz, both for the upper and lower ring of detectors. The measured data are read out using a 12 bit ADC-card. The entire process is controlled via a workstation that sends out the trigger signals to the sources and reads out the detectors.

# 3 Tomographic Reconstruction

## 3.1 Measuring Principle

Each detector measures the attenuation of the X-rays in a thin cone. In the reconstruction this is treated as a thin line. If such a line of mono-energetic $\gamma$- or X-rays is transmitted through a closed system containing a particle-gas two-phase mixture, the number of photons registered per second, $R$, follows from the Lambert-Beer law:

$$R = R_0 exp\left[-\left((1-\alpha)\mu_p + \alpha\mu_g\right)d\right] \tag{1}$$

where $R_0$ is the number of photons registered per second when the system is in vacuum; $\mu_p$ and $\mu_g$ denote the linear absorption coefficient of the particle and gas phase; $\alpha$ is the volume fraction of the gas phase; $d$ is the inner diameter of the system. It should

be noted that the attenuation characteristics of the fluidized bed wall is incorporated in $R_0$. X-ray sources generate a wide spectrum of X-ray energies. The attenuation coefficients, $\mu_p$ and $\mu_g$, are functions of the photon energy $E$. Therefore, a two point calibration is inadequate, as the absorption of the photons of lower energy is much faster. In order to deal with this, we have calibrated all detector individually by placing various amounts of packed powder in between a source and its detectors. The amount of packed powder is put inside the column to ensure that the calibration encompasses the effects of the walls of the column. Furthermore, the calibration includes a completely empty and a completely filled bed. These two calibration points provide the upper and lower limit of the signal. We fitted a smooth function of the form $A_{cal} + B_{cal} \cdot exp\left(-x/C_{cal}\right)$ to the data, with $x$ the distance traveled by the beam through the powder phase. For every detector, an individual curve is obtained, see (14).

## 3.2 Tomographic Reconstruction

We use an Algebraic Reconstruction Technique. Although significantly slower than e.g. Linear Back Projection, algebraic methods offer more flexibility in terms of limited data sets and are more appropriate for the CT configuration system under consideration here. Detailed accounts of reconstruction techniques can be found in (15), (16) or (17). We use the calibration curve to convert the measured line-averaged attenuation into a line averaged solids fraction. We will reconstruct the solids fraction $\alpha(x, y)$ in a pixel representation of the cross-section of the fluidized bed. Here, we use a square pixel array of 55*55 pixels. The cross-section of the fluidized bed exactly fits in this square. All pixels outside the circle have a solids fraction of zero. For a given ray, traveling through the object, the total solids fraction on the line, $p_i$, referred to as *ray sum*, can be estimated as

$$\tilde{p}_i = \sum_{k=1}^{N} W_{ik}\alpha_k \tag{2}$$

with $\alpha_k$ the pixel-based value of the solids fraction distribution and $W_{ik}$ the weighing factor for pixel $k$ for the $i^{th}$ ray through the object. We use a linear weighing matrix $W$. Hence, the weighing factor $W_{ik}$ is the length of ray $i$ through pixel $k$

To reconstruct the image we need to solve the unknown pixel-averaged solids fraction $\alpha_k$ from eq.(2) for $M$ different rays on $N$ pixels. As the number of independent measurements is only 3*30=90 and the number of unknown pixels is easily 1000 or more, the problem is ill-posed. Moreover, there will be measuring noise in the data. The Algebraic Reconstruction Techniques (ART, see e.g. (15)) are designed to minimize the mismatch between the data $\vec{p}$ and $\mathbf{W} \cdot \vec{\alpha}$. They are iterative methods that solves $\vec{p} = \mathbf{W} \cdot \vec{\alpha}$. We use the Simultaneous Algebraic Reconstruction Technique (SART) (18). Instead of sequentially updating the pixels on a ray-by-ray basis, SART simultaneously applies to a pixel the average of the corrections generated by all rays. This offers a reduction in the amplitude of the salt and pepper noise that is usually present in ART. However, it goes at the expense of the computation time.

Still, pepper and salt noise will be present in the images. This can be reduced by using a so-called one-step-late algorithm (see (19)). We invoked an algorithm based on the median root function (suggested first by (20)). It effectively removes pepper and salt noise, but keeps the edges of larger objects sharp enough, see e.g. (14) for full details about the reconstruction algorithm.

# 4 Experimental Results

X-ray sources are inherently noisy. In the present work, we have averaged the data first over one period of the 10 data points and moved in steps of 10 time steps through the data series for each new reconstruction. This obviously reduces the time resolution of the images from 2500 frames per second to 250 frames per second.
Two types of experiments are performed: (i) a cylinder of known size is pulled at constant velocity through the unfluidized bed. From the response of the detectors in the two planes, we can find the time it takes for the cylinder to move from the lower plane to the upper one. As the cylinder velocity is measured independently, we can this way find the distance between the two planes.

X-ray sources are inherently noisy. Therefore, we first denoised the raw data from the cylinder experiments, using a Wavelet-denoising. This is done in Matlab, using the functions 'ddencmp' to decompose and then 'wdencmp' to reconstruct the denoised signal. An example of the original and denoised signal for passage of the cylinder is shown in fig.(2).

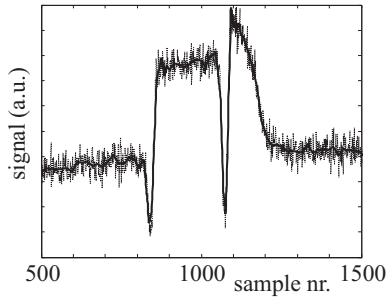


Figure 2: Raw signal (dashed, thin line) and denoised one (solid line).

By comparing either of the two peaks (stemming from the top and bottom of the cylinder) from two corresponding detectors (one in the lower, one in the upper plane), the time of flight can be found. The averages for all three sources are given in fig.(3). The plot shows, that, as expected, the time of flight is a linear function of the inverse of the cylinder velocity. The best linear fit through the data is used as the calibration of the plane-plane distance. It is found to be 1.86cm, which is close to the 2cm-distance based on geometrical arguments.

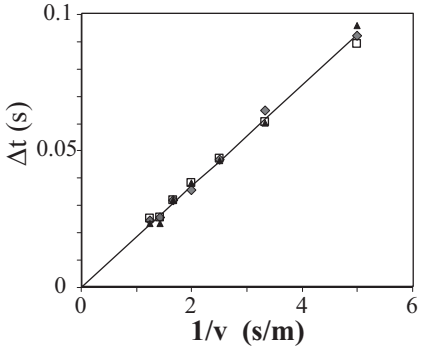


Figure 3: Average time of flight versus 1/v for all three source-detectors.

Next, the bed is set at minimal fluidization. A single capillary (inner diameter 4mm) is inserted into the bed with its exit 132mm above the porous plate of the fluid bed. Additional air flows through this capillary, creating a train of bubbles. These bubbles rise upwards and pass the two measuring planes, where they are detected. Data are

taken for a period of 5 seconds. The raw data are groups in sets of 10 samples and the average of each set is calculated. From these smoothed data reconstructions are calculated. This generates 1250 images, separated by a time interval of 4ms.

We performed a series of experiments with the fluidized bed positioned on a table that can be traversed in the vertical direction. This allows us to perform experiments at various heights above the exit of the capillary, i.e. at 7cm, 17cm and 37cm. The gas flow rate through the capillary was set at 0.56 *l*/s, which is equivalent to a superficial velocity for the fluid bed of 1.34cm/s. The velocity of the gas inside the capillary is some 44m/s. Hence, we are blowing a jet of gas into the fluidized bed that breaks up in small bubbles. We took measurements during 5 seconds. The raw data were used to reconstruct the bubbles. Furthermore, they were denoised and the velocity of the individual bubbles was found from the denoised time-series. In 5 seconds measuring interval, we registered 45 bubbles for the case the measuring plane was 7cm above the capillary exit, 22 for a measuring height of 17cm and 8 for the 37cm case. The reconstructed images are stacked creating a 3D picture, see fig.(4) for the 37cm height.

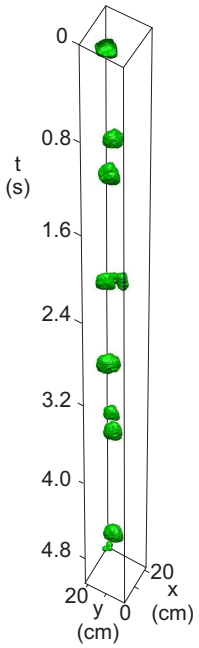


Figure 4: Reconstruction of the bubble train passing the measuring plane 37cm above the capillary exit.

The figure has time as the virtual axis and hence the size of a bubble should be interpreted with care: its vertical dimension is in seconds. As we have measured the velocity of each individual bubble that passes the two measuring planes, we can convert the vertical dimension of each bubble from passage time to actual height. However, we can not do the same for the distance between two consecutive bubbles as we only know the bubble velocity at the moment of passage of the measuring plane and not the velocities of the two bubbles at the same time. Nevertheless, from the bubble velocity and the reconstructed and stacked images, we can find now the bubble height and the bubble volume. From the latter, we compute the bubble equivalent diameter: $D_{eq} \equiv \left(\frac{6}{\pi} V_{bub}\right)^{1/3}$. We expect that the bubbles at the lower heights above the capillary exit are smaller and are in the process of coalescing. This would mean, that the bubble sizes are smaller at smaller heights and that the bubble velocity would show a wide range as trailing bubbles are accelerated into the wakes of leading ones. Fig.(5) shows the equivalent bubble diameter versus the bubble velocity for the two measuring heights.

As we see in the figure, at the lower height the bubbles are significantly smaller than at the higher position. Roughly speaking, bubbles 17cm above the exit are some 5.5cm in equivalent diameter, whereas at 37cm above the exit their average size is about 7.6cm. These numbers are reasonable: if two bubbles of 5.5cm equivalent diameter coalesce while keeping the total volume constant, the new bigger bubble will have an equivalent diameter of 6.9cm. Note, that at 37cm the bubble velocity spans a narrow range. The bubble-bubble distance has become so large, that the bubble-bubble interaction is weak and trailing bubbles hardly feel an accelerating force towards the leading one. Further, we see that the initial velocity of the bubbles is high: at 7cm above the exit of the capillary their velocity is higher than at higher measuring positions. This is evidently caused by the high velocity of the injected gas.

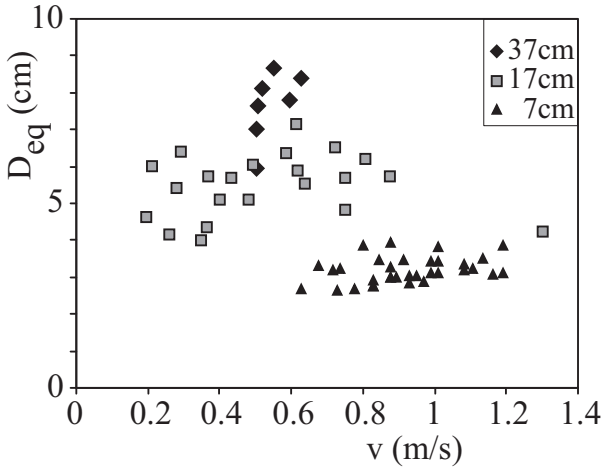


Figure 5: Equivalent diameter at three different heights.

## 5 Concluding Remarks

In this paper, we present experiments using our double Xray CT-scanner. We could measure bubbles that have sizes of some 2.5cm rising up in a bubble train through a fluidized bed at minimal fluidization conditions. The scanner is able to provide data on individual bubbles: their size, volume and velocity. Especially the latter is important as the scanner measures the bubbles passing a plane. Without the velocity, the vertical dimension of the bubbles would be time, rather than length. We performed a calibration experiment, that allows us to accurately find the relation between time of flight from the lower measuring plane to the higher one and the velocity of objects.
From experiments of a jetting capillary, we could observe bubbles relatively close to the injection point, where their velocity is much larger than the terminal velocity based on their size. We noticed that higher in the column the bubble slow down and, as expected, increase in size. From the data we could draw the conclusion, that our scanner is accurate enough to provide quantitative data on bubbles in a fluidized bed of 23cm diameter. It shows that this technique can compete with other tomographic techniques applied to fluidized beds.

## References

[1] N. Reinecke and D. Mewes. Recent developments and industrial research applications of capacitance tomography. *Meas. Sci. & Techn.*, 7:233, 1996.

[2] F. T. Kühn, J. C. Schouten, R. F. Mudde, C. M. Van den Bleek, and B. Scarlett. Analysis of chaos in fluidization using electrical capacitance tomography. *Meas. Sci. & Techn.*, 7:361, 1996.

[3] M. S. Beck, T. Dyakowski, and R. A. Williams. Process tomography - the state of the art. *Trans. Inst. Meas. and Control*, 20(4):163–177, 1998.

[4] W. Warsito and L.-S. Fan. Neural network based multi-criterion optimization image reconstruction technique for imaging two - and three-phase flow systems

using electrical capacitance tomography. *Meas. Sci. Techn.*, 12(12):2198–2210, 2001.

[5] W. Warsito and L.-S. Fan. Dynamics of spiral bubble plume motion in the entrance region of bubble columns and three-phase fluidized beds using 3d ect. *Chem. Eng. Sci.*, 60:6073–6084, 2005.

[6] L.F. Gladden, L.D. Anadon, C.P. Dunckley, M.D. Mantle, and A.J. Sederman. Insights into gas-liquid-solid reactors obtained by magnetic resonance imaging. *Chem. Eng. Sci.*, 62 (24):6969–6977, 2007.

[7] M.P. Dudukovic. Opaque multiphase reactors: Experimentation, modeling and troubleshooting. *Oil & Gas Sci. Tecn.*, 55(2):135–158, 2000.

[8] S.B. Kumar, D. Moslemian, and M.P. Dudukovic. A $\gamma$-ray tomographic scanner for imaging voidage distribution in two-phase flow systemss. *Flow Meas. Instr.*, 6 (1):61–73, 1995.

[9] S.B. Kumar, D. Moslemian, and M.P. Duduković. Gas holdup measurments in bubble columns using computed tomography. *AIChE J.*, 43:1414, 1997.

[10] K.A. Shollenberger, J.R. Torczynski, D.R. Adkins, T.J. O'Hern, and N.B. Jackson. Gamma-densitometry tomography of gas holdup spatial distribution in industrial-scale bubble columns. *Chem. Eng. Sci.*, 52 (13):2037–2048, 1997.

[11] W.K. Mudde, R.F.and Harteveld, H.E.A. van den Akker, T.H.J.J. van der Hagen, and H. van Dam. Gamma radiation densitometry for studying the dynamics of fluidized beds. *Chem. Eng. Sci.*, 54:2047–2054, 1999.

[12] M. Bieberle and U. Hampel. Evaluation of a limited angle scanned electron beam x-ray ct approach for two-phase pipe flows. *Meas. Sci. Technol.*, 17:2057–2065, 2006.

[13] M. Bieberle, F. Fischer, E. Schleicher, U. Hampel, D. Koch, K.S.D.C. Aktay, H.-J. Menz, and H.-G. Mayer. Ultrafast limited-angle-type x-ray tomography. *Appl. Phys. Lett.*, 91(12):123516, 2007.

[14] R. F. Mudde, J. Alles, and T.H.J.J. Van der Hagen. Feasibility study of a time-resolving x-ray tomographic system. *Meas. Sci. & Techn.*, 19:085501, 2008.

[15] R. A. Brooks and G. DiChiro. Principles of computer assisted tomography (cat) in radiographic and radioscopic imaging. *Phys. Med. Biol.*, 21:689, 1976.

[16] G. T. Herman. *Image reconstruction from projections - the fundamentals of computerized tomography*. Academic Press, 1980.

[17] M. Kak and M. Slaney. *Principles of computerized tomographic imaging*. IEEE Press, New York, 1988.

[18] A. H. Andersen and A. C. Kak. Simultaneous algebraic reconstruction technique (sart): a superior implementation of the art algorithm. *Ultrasonic Imaging*, 6:81–94, 1984.

[19] P. J. Green. Bayesian reconstruction from emmission tomography data using a modified em algorithm. *IEEE Trans. on Med. Imag.*, 9:84–93, 1990.

[20] S. Alenius and U. Ruotsalainen. Bayesian image reconstruction for emmission tomography based on median root prior. *Eur. J. of Nucl. Med.*, 22, 1997.